6-2017

Numerical Simulation of the Phase Space of Jupiter-Europa System Including the Effect of Oblateness

Vinay Kumar
University of Delhi

Beena R. Gupta
University of Delhi

Rajiv Aggarwal
University of Delhi

Recommended Citation

Numerical Simulation of the Phase Space
of Jupiter-Europa System Including the Effect of Oblateness

[1]**Vinay Kumar,** [2]**Beena R Gupta &** [3]**Rajiv Aggarwal**

[1]Department of Mathematics
Zakir Husain Delhi College
University of Delhi
Delhi, India
vkumar@zh.du.ac.in
&
[2]Department of Mathematics
Lakshmibai College
University of Delhi
Delhi, India
beenaguptalbc@gmail.com
&
[3]Department of Mathematics
Siri Aurobindo College
University of Delhi
Delhi, India
rajiv_agg1973@yahoo.com

Abstract

We have numerically investigated the phase space of the Jupiter-Europa system in the framework of a Circular Restricted Three-Body Problem. In our model, Jupiter is taken as oblate primary. We have considered time-frequency analysis (TFA) based on wavelets and the Poincare Surface of Section (PSS) for the characterization of orbits in the Jupiter-Europa model. We have exploited both cases: a system with and without considering the effect of oblateness. Graphs (ridge-plots) explaining the phenomenon of resonance trapping, a difference between chaotic sticky orbit and the non-sticky orbit, and periodic and quasi-periodic orbit are presented. Our results of Poincare surfaces of the section of the Jupiter-Europa system (with and without the effect of

oblateness) reveal the impact of oblateness of Jupiter as reducing parameter for regular and chaotic regions. Time-frequency analysis based on wavelets is comparatively fast and is suitable for the identification and characterization of the different type of trajectories in the nonlinear dynamical system.

Keywords: Jupiter-Europa System; Time-frequency analysis; Poincare Surface of Section; Effect of Oblateness; Wavelet Analysis

MSC 2010 No.: 37M10, 37M05, 70F07, 34C60

1. Introduction

We know that the Circular Restricted Three-Body Problem (CRTBP) is one of the most important topics in celestial mechanics and dynamical astronomy. The CRTBP describes the motion of an infinitesimal body moving under the gravitational effect of two primary-bodies with finite masses which move in circular orbits around their common center of mass. It is assumed that the third body does not influence the motion of the two primaries. This model has numerous applications in the field of stellar systems, celestial mechanics, galactic dynamics, artificial satellites, molecular physics and chaos theory, and therefore this is a field of active research (Zotos (2015)). In general, the shapes of the two primaries in the classical version of CRTBP is assumed to be spherically symmetric. However, we know that several celestial bodies, such as Saturn and Jupiter, are oblate or even triaxial. The oblateness of a celestial body has significant effect on the motion of the third body in CRTBP. The study of oblateness effect is explained in Zotos (2015), Kalantonis et al. (2005, 2006, 2008), Kalvouridis et al. (2012), Markellos et al. (1996, 2000), Perdiou et al. (2012), Sharma el al. (1979, 1981, 1986, 1987, 1989, 1990), Singh et al. (2012, 2013), and Subba Rao et al. (1988, 1997). The oblateness of Neptune is included in Stuchi et al. (2008) regarding the dynamics of a spacecraft in the Neptune-Triton system. The effect of oblateness of Saturn on the Saturn-Titan system through PSS can be found in Beevi et al. (2012).

In this paper, we have numerically investigated the effect of oblateness on the phase space of the Jupiter-Europa system using the Poincare surface of section. After this, we have applied time-frequency analysis (based on wavelets) to identify periodic and quasiperiodic orbits in this system under the effect of oblateness. We have simulated this system without considering the impact of oblateness too. Time-frequency analysis based on wavelets and its applications to Circular Restricted Three Body Problem is discussed in the work of Beena et al. (2016), Pourtakdoust et al. (2014), Saha et al. (2008), and Vela-Arevalo et al. (2004). The application of wavelets can be found in the work of Chandre et al. (2003), Gupta et al. (2015), and Michtchenko et al. (1996). The drawback of these two methods (TFA based on wavelets and PSS) is its programming. TFA based on wavelets and PSS are comparatively fast and are an efficient approach.

The method of TFA based on wavelets is computed via two processes. First is TFA based on the amplitude of CWT, and the other relies on the phase of CWT. Concept and applications of TFA

Kumar et al.: Numerical Simulation of the Phase Space of Jupiter-Europa

AAM: Intern. J., Vol. 12, Issue 1 (June 2017)   481

based on the amplitude of CWT can be found in the work of Chandre et al. (2003), Michtchenko et al. (1996), and Todorvska (2001). On the other hand, concept and applications to nonlinear dynamical systems of TFA based on the phase of CWT can be seen in the work of Deplart et al. (1992) and Vela-Arevalo et al. (2004). It is suggested in the work of Deplart et al. (1992) and Vela-Arevalo et al. (2004) that TFA based on the phase of CWT is the comparatively efficient tool to study any time series signal or non-linear dynamical systems.

Poincare surface of section is also a useful instrument for the study of nonlinear dynamical systems with two degrees of freedom. Visualization of PSS gives the whole picture of the phase space structure. In the case of nonlinear dynamical systems of three degrees of freedom, PSS is less straightforward. In that case, TFA based on wavelets solves the problem. Clear visualization and determination of time interval of resonance trapping of the chaotic trajectory are possible with TFA based on wavelets. Different types of trajectories such as periodic, quasiperiodic, and chaotic are computed in comparatively less time and effort. This combination can identify sticky (chaotic) orbits, i.e. the orbit that behaves as almost regular orbit for an extended period and then escapes to chaotic domain (Freistetter (2000)).

We have organized this paper as follows. In Section 2, the brief description of the configuration of Jupiter-Europa-satellite is given. In Section 3, we present the method of implementation of TFA based on wavelets in Matlab and PSS in Mathematica. Results regarding the application of TFA based on wavelets and PSS to the nonlinear model are discussed in Section 4. Conclusions drawn by results are shown in Section 5. We end this paper in an Appendix in which we have presented different periodic orbits (Figures 16, 17) obtained using TFA based on wavelets.

2.   Jupiter-Europa-Satellite System

We consider the Jupiter-Europa-satellite system in the framework of Circular Restricted Three-Body Problem. In this model, we take Jupiter as an oblate spheroid. We have considered Jupiter and Europa as two primaries moving around their center of mass in circular orbits due to the influence of their mutual gravitational attraction. A satellite is considered as an infinitesimal mass (attracted by the primaries, but not affecting their motion) which moves on the plane defined by the primaries.

We have assumed the following things:

1. The distance between primaries does not change and is taken equal to one.
2. We take the sum of the masses of the primaries as one.
3. To make the gravitational constant unity we consider the unit of time.
4. After the normalization of time and position coordinates, the system has only one parameter μ, which is the ratio between the mass of one primary to the total mass of the system. For the Jupiter-Europa system with masses m_J and m_E, the mass parameter is defined as

$$\mu = \frac{m_E}{m_J + m_E} = 0.002521721. \ \left(\text{As} \ \mu = \frac{m_2}{m_1 + m_2}, \ \text{where} \quad m_2 < m_1.\right)$$
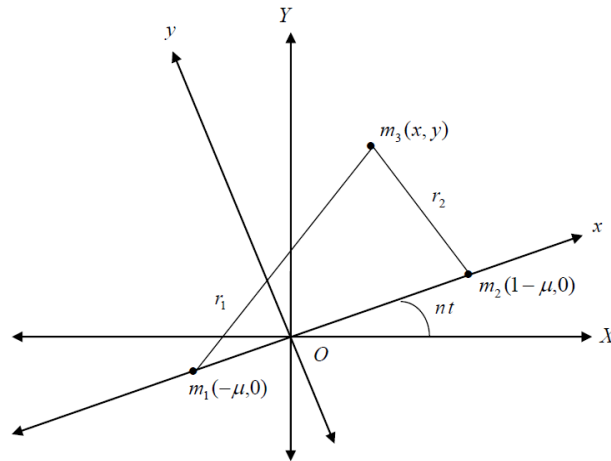
Figure 1:   Configuration of Jupiter-Europa System in the framework of the Circular Restricted Three-Body Problem

We choose synodic coordinate system as reference frame. The origin is at $(0,0)$, and the center of the primaries are located at $(-\mu, 0)$ and $(1-\mu, 0)$ respectively. Total effective potential of this system including effect of oblateness can be defined as Sharma et al. (1976).

$$V(x,y) = -\frac{1-\mu}{r_1} - \frac{\mu}{r_2} - \frac{(1-\mu)A_3}{2r_1^3} - \frac{n^2}{2}(x^2 + y^2), \tag{1}$$

where

$$r_1^2 = (x+\mu)^2 + y^2, \quad r_2^2 = (x-1+\mu)^2 + y^2, \tag{2}$$

$$n^2 = (1 + 3A_1/2), \text{ (Here `n' is the mean motion.)} \tag{3}$$

where A_1 is the coefficient of oblateness which is defined as

$$A_1 = \frac{RE^2 - RP^2}{5R^2} = 0.000185783652352, \tag{4}$$

where RE and RP are the equatorial radius and polar radius of the oblate body, respectively. R is the distance between the centers of two primaries. Equations of motion for the the above model are

$$\ddot{x} - 2n\dot{y} = -\frac{\partial V(x,y)}{\partial x}, \qquad \ddot{y} + 2n\dot{x} = -\frac{\partial V(x,y)}{\partial y}. \tag{5}$$

The system (5) admits a well known Jacobi integral which is defined as

$$J(x,y,\dot{x},\dot{y}) = \frac{1}{2}(\dot{x}^2 + \dot{y}^2) + V(x,y) = E. \tag{6}$$

We have considered the value of energy constants for the Jupiter-Europa system without oblateness and with oblateness as 3.067 and 3.13, respectively. There are five stationary points among which three are unstable, and two are stable in both cases. To start with PSS and TFA based on wavelets, we must have an idea about the regions of motion for Jupiter-Europa system (with or without oblateness). The region of motion gives us the idea about the range of initial conditions in

Kumar et al.: Numerical Simulation of the Phase Space of Jupiter-Europa

AAM: Intern. J., Vol. 12, Issue 1 (June 2017)   483

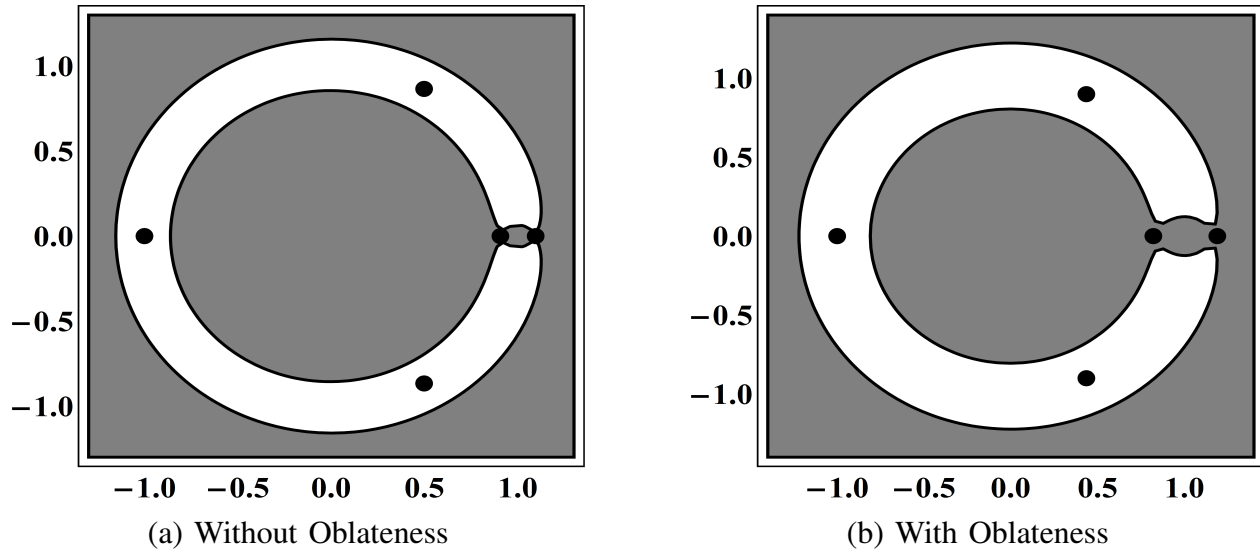(a) Without Oblateness   (b) With Oblateness

Figure 2:   Regions of motion (colored) for Jupiter-Europa system without oblateness and with oblateness at $E = 3.067$ and $E = 3.13$ respectively

which the equations of motion given by (5) and (6) will be integrated to provide the trajectories, and these trajectories will be tested using TFA-based phase of the continuous wavelet transform.

From (6), we can compute $\dot{y}(0)$ depending upon $(x(0), y(0), \dot{x}(0))$ which is given as follows,

$$\dot{y} = \sqrt{2E - (\dot{x})^2}. \tag{7}$$

Regions of motion are plotted using Mathematica. We have plotted the graph for $(2E - (\dot{x})^2) \geq 0$. In Figure 2, we have plotted regions of motion for both cases. Due to an impact of oblateness, we find that the neck-shaped area obtained at energy constant 3.13 whereas without oblateness effect the neck-shaped region obtained at 3.067. Also, the forbidden region of motion has increased due to oblateness effect. The whole area of motion is divided into three parts: interior, boundary, and exterior regions. The third body can move anywhere except forbidden regions of motion.

3.   Time-frequency analysis based on phase of CWT

The continuous wavelet transform is defined in terms of Ψ, called mother wavelet, expressed as

$$L_\Psi f(a, b) = \frac{1}{\sqrt{a}} \int_{-\infty}^{\infty} f(t)\, \overline{\Psi}\left(\frac{t - b}{a}\right)\, dt. \tag{8}$$

The function $\Psi \in L^2(R)$ must have compact support or decay rapidly to 0 for t tending to ∞ or $-\infty$. The wavelet transform depends on two parameters (a,b): a is called the scale and b the time parameter. The wavelet transform produces a complex surface as a function of the variables a and b. A common representation of this surface is known as density plot of the modulus of $L_\Psi f(a, b)$, with b as horizontal axis (time) and $\log(a)$ as the vertical axis. However, since the frequency ω

is proportional to the inverse of the scale $1/a$, we opted for the frequency ω as the vertical axis. The mother wavelet that we use throughout this work is known as the Morlet-Grossman wavelet is defined in Beena et al. (2015),

$$\Psi(t) = \frac{1}{\sigma\sqrt{2\pi}} e^{\ i2\pi\eta t} e^{-\frac{t^2}{2\sigma^2}}. \tag{9}$$

The procedure for finding instantaneous frequency using phase of continuous wavelet transform can be seen in Gupta et al. (2016), Todorovska (2001), and Vela-Arevalo et al. (2004).

3.1   Difference between Windowed Fourier Transform (WFT) and Wavelet Transform (WT)

The drawback of Windowed Fourier Transform is having its fixed window, which is not in the case of the wavelet transform. In the case of WFT, the length of the window is set (say σ) and therefore any event (trapping, transition, etc.) happening on short time-scales (i.e., less than σ) or with small frequencies (less than $1/\sigma$) is missed by this method. On the contrary, WT method adapts the length of the window according to the frequencies. In the case of quasiperiodic trajectories, WFT and WT are exactly same. But for chaotic trajectories, where the variation of frequency takes place, WT gives better time-frequency resolution (Chandre et al. (2003)).

3.2   Drawbacks of SALI, CD and LLCE

The computation of these indicators needs the solution of the equation of motion and the first variational equations. This additional computational effort is not easy in case of the system having large dimension. Their algorithms take a longer time to execute (due to a large number of equations). Also, they don't give much qualitative information of phase space structure (e.g., if a trajectory is resonant or non-resonant) (Gupta et al. (2016)).

3.3   Implementation of Wavelet-ridges in Matlab and Poincare surface of section in Mathematica

The algorithm for computing ridges from the phase of the continuous wavelet transform is already explained in Deplart et al. (1992), Todorovska (2001) and Vela-Arevalo et al. (2004). Programs based on the algorithm can be made with the help of Wavelab routines written in Matlab (Wavelab). Computation of CWT is done by Wavelab routines written in Matlab. For PSS, we have used Runge-Kutta 4-5 variable step size integrator method. The initial condition for PSS is taken as $(x(0), 0, 0, \dot{y}(0))$. Here $x(0)$ is taken on x-axis at the step size 0.01 in the permissible region (Figure 2). PSS is drawn in Mathematica.

We use the following steps for the computation of instantaneous frequency plot (ridge-plot):

1. Observation of the Poincare-plots for thousands of initial conditions, and then we choose selected initial conditions reflecting different aspects of motion.
2. Integration of the equations of motion given in (5) for the time interval $T = 1$ to 32768.
3. The computation of the instantaneous frequency $\omega(t)$ from $Z(t)$ using the Wavelab routines. Construction of the signal from the numerical solutions $(x(t), y(t), \dot{x}(t), \dot{y}(t))$ of equations

Kumar et al.: Numerical Simulation of the Phase Space of Jupiter-Europa

AAM: Intern. J., Vol. 12, Issue 1 (June 2017)   485

of motion (5) is given as

$$Z(t) = X(t) + iY(t) = \exp^{-it}(x(t) + iy(t)). \tag{10}$$

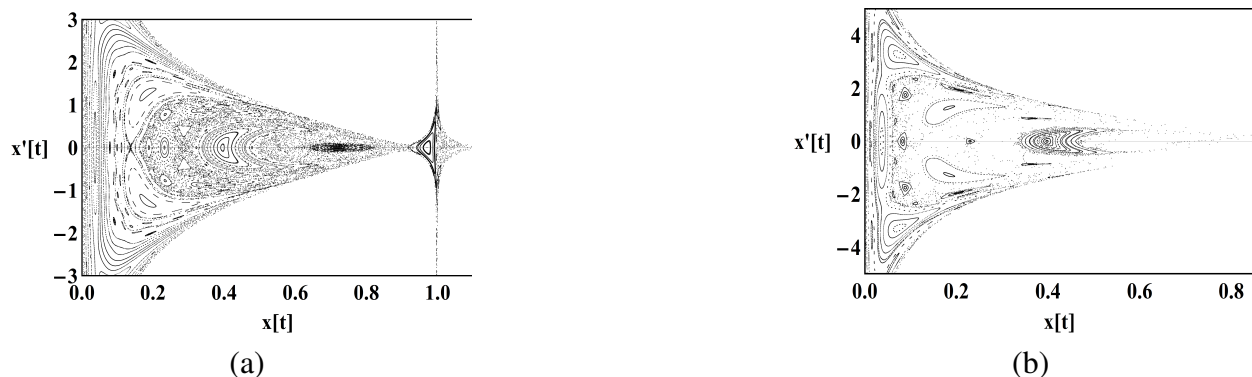## 4. Application of PSS and TFA based on wavelets to Jupiter-Europa system

(a)   (b)

Figure 3:   (A) PSS of Jupiter-Europa system without influence of oblateness at Energy Constant $C = 3.067$ (B) PSS of Jupiter-Europa system under influence of oblateness ($A = 0.000185783652352$) at Energy Constant $C = 3.067$
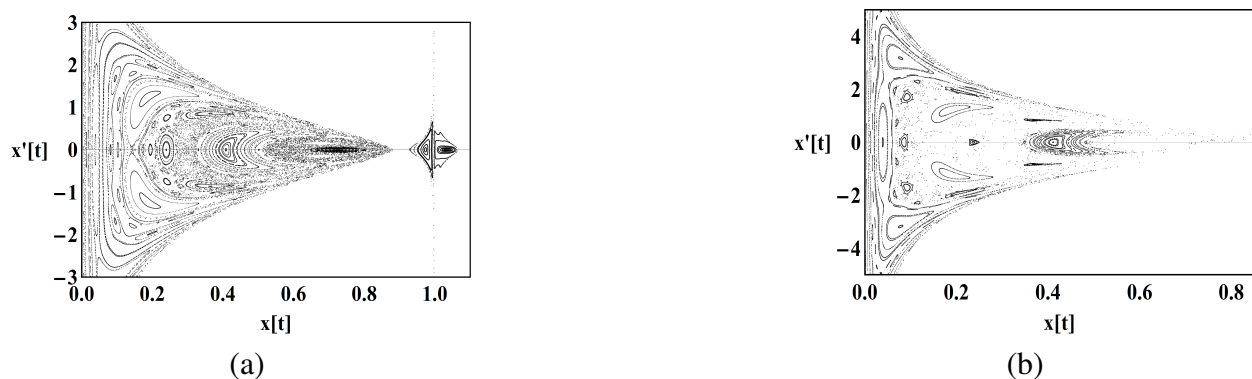

(a)   (b)

Figure 4:   (A) PSS of Jupiter-Europa system without influence of oblateness at Energy Constant $C = 3.08$ (B) PSS of Jupiter-Europa system under influence of oblateness ($A = 0.000185783652352$) at Energy Constant $C = 3.08$

At first, we apply the method of the Poincare surface of section to analyze the effect of the oblateness on the phase space of Jupiter-Europa system. We have done it in two ways:

1. In Figures 3, 4, 11, and 12, we observe PSS at energy constants 3.067, 3.08, 3.09 and 3.1, respectively. The oblateness parameter of Jupiter is taken in these figures. In figures (above mentioned), first PSS is without oblateness and second is including the effect of

oblateness in all figures. All graphs related to the Poincare surfaces of section are drawn in Mathematica. We see that the area of the chaotic region, as well as regular region, has reduced significantly in the case when Jupiter is taken as the oblate body.

2. We have also examined the effect of oblateness parameter of Jupiter by taking it in the interval $[0.0001, 0.000001]$ (Figures 13, 14, and 15). In all these figures, we fix the energy constants ($C = 3.067$). We decrease the value of the oblateness parameter like 0.0001, 0.00001 and 0.000001 respectively. When we reduce the oblateness parameter, the area of the phase space filled with chaotic and regular regions increases. Here, we note the significant change in the phase space structure of this system under the influence of the oblateness parameter.

Table I: Sample of orbits for the Jupiter-Europa system (2D) and the respective results. The indicator "Time" stands for the execution time in sec of the program on the computer

No.	(x0 , y0, $\dot{x}0$, $\dot{y}0$)	Energy Const.	Time (Ridge-Plot)	Type of Orbit
1	(0.453, 0, 0, 1.2367)	3.067	13.16	Periodic
2	(0.95, 0, 0, 0.1966)	3.067	13.59	Quasi-Periodic
3	(0.871, 0, 0, 0.1336)	3.067	14.25	Chaotic sticky
4	(0.31, 0, 0, 1.85)	3.067	13.59	Chaotic nonsticky
5	(-0.51, 0, 0, 1.0318)	3.13	14.65	Periodic (Including Oblate)
6	(-0.61, 0, 0, 0.7276)	3.13	13.65	Quasi-Periodic (Including Oblate)

In Table I, we have presented a sample of six trajectories showing different aspects of motion in the Jupiter-Europa system with and without an effect of oblateness. The first four trajectories are without oblateness effect, and the other two are under the influence of oblateness. Different examples of periodic orbits drawn with the help of TFA based on wavelets are given in the Appendix (Figures 16, 17). We characterize the different type of trajectories concerning the evolution of frequency with respect to time. Periodic and Quasiperiodic trajectories are characterized by constant frequencies. Variation in frequency with respect to time represents chaotic trajectory. The time taken for the execution of the program for TFA based on wavelets and PSS is negligible in comparison to the other chaos indicators such as SALI, LLCE, and CD (Racoveanu (2014)).

4.1   Jupiter-Europa system without oblateness effect

1. The first orbit is at initial condition $(0.453, 0, 0, 1.2367)$, shown in Figure 5. We see that the Phase-portrait (Figure 5(A)) reflects the regularity of orbit. In Ridge-plot, we observe constant ridge (Figure 5(B)) throughout the time interval. Thus, we characterize this orbit as periodic orbit.

2. The second orbit is at initial condition $(0.95, 0, 0, 0.1966)$ in Figure 6. Phase-portrait at this condition represents a torus shape trajectory. In ridge-plot, we observe two frequencies among which, first is constant and second sub-frequency has little variation. By ridge-plot, we call this orbit as Quasiperiodic orbit.

3. The third orbit is at initial condition $(0.871, 0, 0, 0.1336)$ in Figure 7. From the Phase-portrait, we observe that the trajectory follows interior region and escape to the external region of motion (see Figure 7(A)). We can conclude that the orbit is not regular. But in the ridge-plot

Kumar et al.: Numerical Simulation of the Phase Space of Jupiter-Europa

AAM: Intern. J., Vol. 12, Issue 1 (June 2017)   487

(Figure 7(B)), we see that the trajectory is trapped up to time unit $T = 17000$ units and after that, it becomes highly irregular. It indicates the resonance trapping of a chaotic trajectory from time $T = 1$ to $T = 16000$. Since this trapping is more than 10000-time units, we call it sticky orbit.

4. This sample of an orbit is taken at initial condition (0.31, 0, 0, 1.85) in Figure 8. In the Phase-portrait, we observe highly disordered trajectory. In ridge-plot (Figure 7), we observe that the ridges are entirely discontinuous. These small discontinued ridges present the strongly chaotic trajectory.

4.2 Jupiter-Europa system under the influence of oblateness

1. The fifth orbit is taken at initial condition (-0.51, 0, 0, 1.0318) displayed in Figure 9. From the phase portrait (Figure 8(A)) we conclude that the orbit is regular. In ridge-plot, we observe constant frequencies characterizing periodic orbit.

2. The last orbit is taken at initial condition (-0.61, 0, 0, 0.7276) in Figure 10. From the Phase-portrait (Figure 9(A)) as described in the first case, it is clear that the orbit is regular. In ridge-plot (Figure 9(B)) we conclude that orbit is quasiperiodic.

   Note: Phase-portraits of different periodic orbits in both cases are given in Appendix. We have checked all orbits using time-frequency analysis and by time-frequency landscape (Ridge-plots) obtained using TFA based on wavelets.

(a) Phase-portrait   (b) Ridge-Plot

Figure 5: Phase-portrait and Ridge-plot of periodic orbit at initial condition (0.4530, 0, 0, 1.2367)

(a) Phase-portrait   (b) Ridge-Plot

Figure 6: Phase-portrait and Ridge-plot of Quasi-periodic orbit at initial condition (0.95, 0, 0, 0.1966)

(a) Phase-portrait   (b) Ridge-Plot
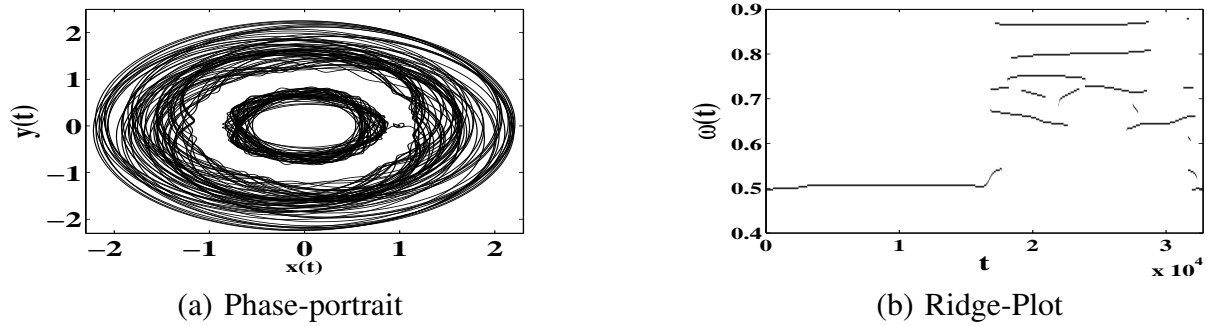
Figure 7:   Phase-portrait and Ridge-plot of chaotic sticky orbit at initial condition (0.871, 0, 0, 1.336)

(a) Phase-portrait   (b) Ridge-Plot
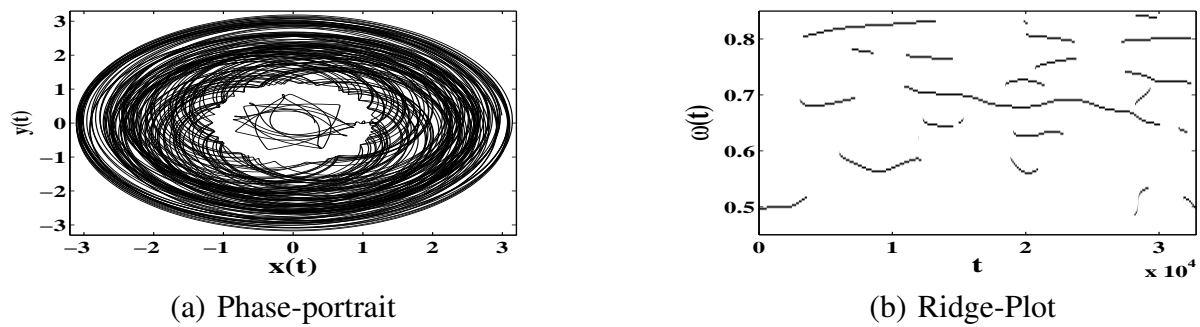
Figure 8:   Phase-portrait and Ridge-plot of chaotic non-sticky orbit at initial condition (0.3100, 0, 0, 1.8500)
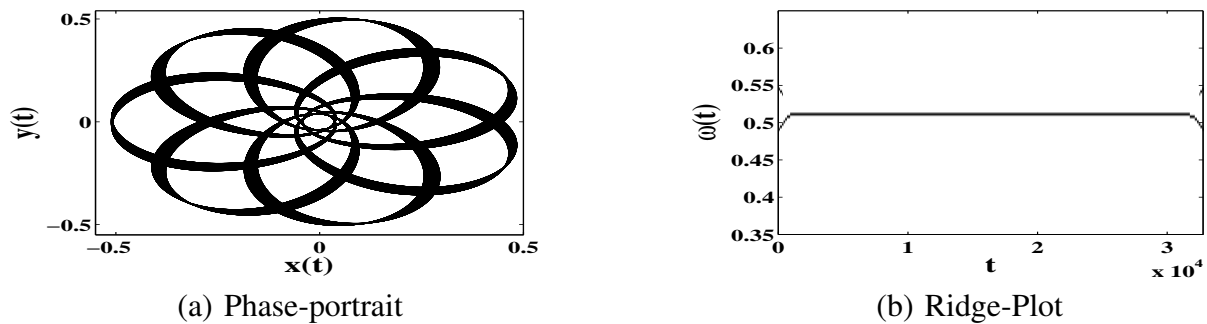

(a) Phase-portrait   (b) Ridge-Plot

Figure 9:   Phase-portrait and Ridge-plot of periodic orbit when one primary is oblate at initial condition (-0.5100, 0, 0, 1.0318)

Kumar et al.: Numerical Simulation of the Phase Space of Jupiter-Europa

AAM: Intern. J., Vol. 12, Issue 1 (June 2017)											489

(a) Phase-portrait
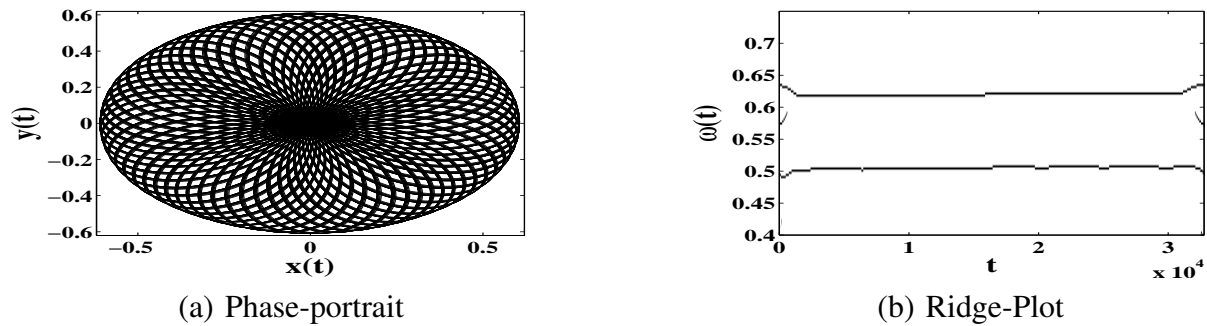
(b) Ridge-Plot

Figure 10: Phase-portrait and Ridge-plot of quasi-periodic orbit when one primary is oblate at initial condition (-0.6100 0 0 0.7276)

5. Conclusion

The present study aims to establish the combination of two methods, PSS and TFA, based on wavelets as an important numerical tool to study the quantitative and qualitative aspect of phase space structure of the nonlinear dynamical systems. We have compared with the combination of three other methods, LLCE, SALI, and CD (Racoveanu (2014)). We have considered the Jupiter-Europa system including the effect of oblateness as a test model. Computation time and effort taken by PSS and TFA based on wavelets is negligible in comparison to the other proposed combination. Thus, our proposed combination is useful for the study of nonlinear dynamical systems in the following manner:

1. The oblateness parameter of Jupiter has a significant impact on the phase space (Figures 3, 4, 11, 12, 13, 14, and 15) as it lessens the regions of motion and also the area covered by of regular and chaotic trajectories in Poincare surfaces of section as well.

2. We have successfully characterized periodic, quasi-periodic, chaotic non-sticky orbit, and chaotic sticky orbits with this combination. The difference between periodic and quasiperiodic, chaotic sticky and chaotic non-sticky, regular and chaotic trajectories is apparent from the ridge-plots (time-frequency landscape).

3. Computational time and effort is less in comparison to other methods. Various chaos indicators (for, e.g., SALI, LLCE, and CD (Todorovska (2001)) require 30 minutes or even more for execution of algorithms whereas this combination needs less than 1 minute. (See Table 1)

4. One of the most important aspects of the chaotic trajectories is the trapping of these trajectories in resonance islands and then their escape to chaotic regions. In Figure 7, we observe the resonance trapping of the trajectory for the time interval $[1, 17000]$. After that, the third body escapes to the chaotic region.

5. The analytical approach for the computation of the periodic orbits in CRTBP is useful and it also involves some complex calculations. On the other hand, TFA based on wavelets require less effort and less computations. We have shown some periodic orbits (Figures 16, 17) in the presence and absence of the effect of oblateness of Jupiter in the Jupiter-Europa system.

(a)   (b)
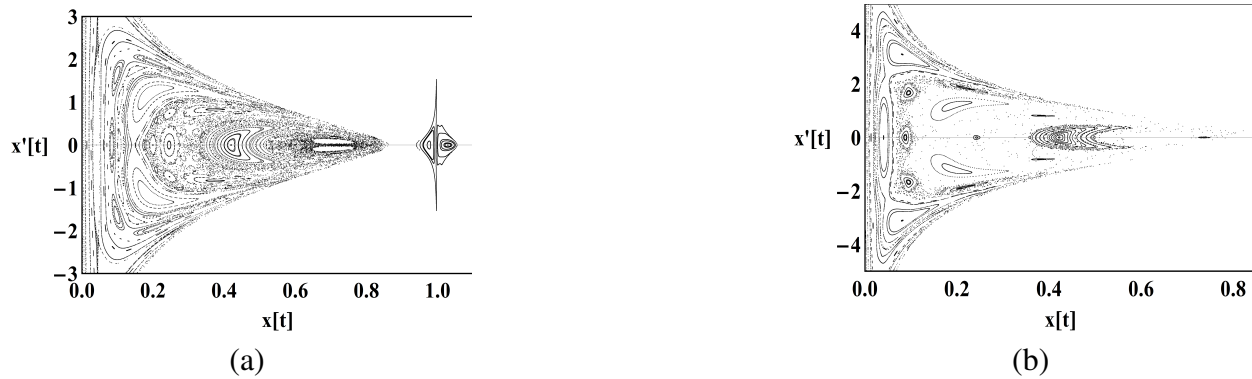
Figure 11: (A) PSS of Jupiter-Europa system without influence of oblateness at Energy Constant $C = 3.09$ (B) PSS of Jupiter-Europa system under influence of oblateness ($A = 0.000185783652352$) at Energy Constant $C = 3.09$
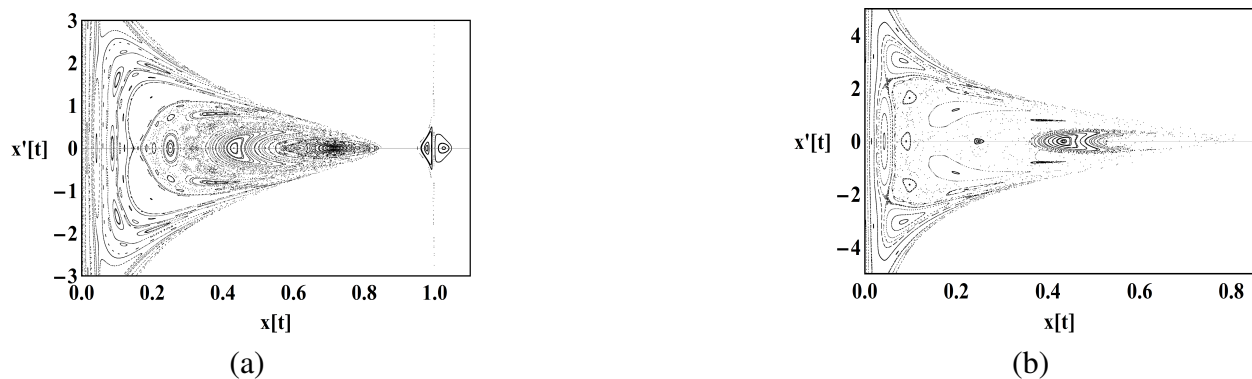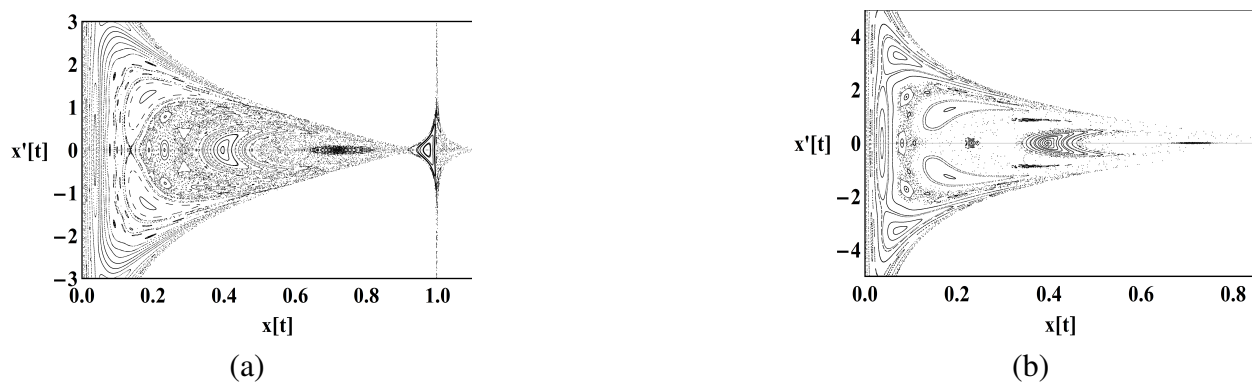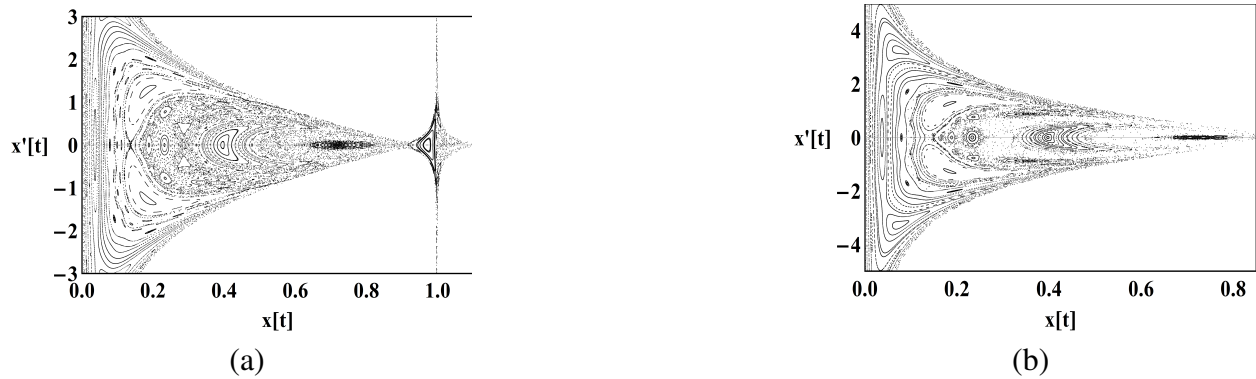

(a)   (b)

Figure 12: (A) PSS of Jupiter-Europa system without influence of oblateness at Energy Constant $C = 3.1$ (B) PSS of Jupiter-Europa system under influence of oblateness ($A = 0.000185783652352$) at Energy Constant $C = 3.1$

(a)   (b)

Figure 13: (A) PSS of Jupiter-Europa system without influence of oblateness at Energy Constant $C = 3.067$ (B) PSS of Jupiter-Europa system under influence of oblateness ($A = 0.0001$) at Energy Constant $C = 3.067$
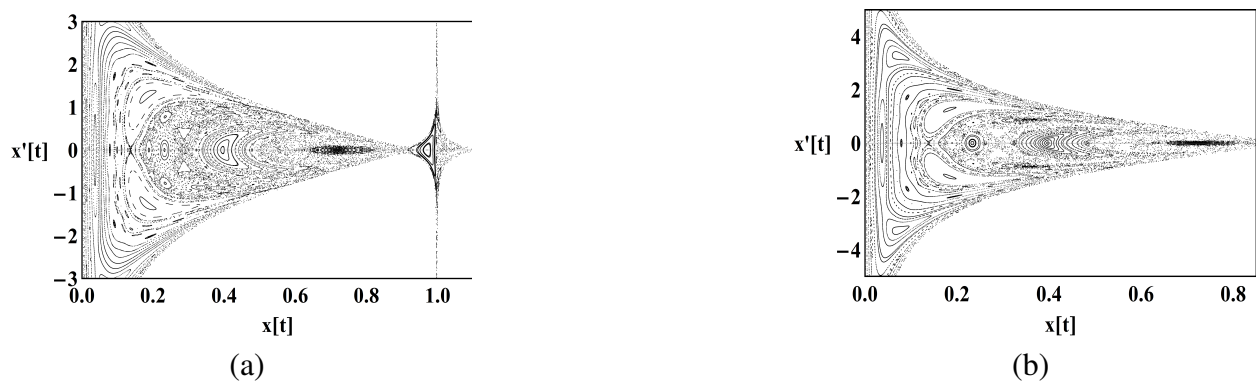
Kumar et al.: Numerical Simulation of the Phase Space of Jupiter-Europa

AAM: Intern. J., Vol. 12, Issue 1 (June 2017)   491

(a)   (b)

Figure 14: (A) PSS of Jupiter-Europa system without influence of oblateness at Energy Constant
$C = 3.067$ (B) PSS of Jupiter-Europa system under influence of oblateness ($A = 0.00001$) at Energy Constant $C = 3.067$

(a)   (b)

Figure 15: (A) PSS of Jupiter-Europa system without influence of oblateness at Energy Constant
$C = 3.067$ (B) PSS of Jupiter-Europa system under influence of oblateness ($A = 0.000001$) at Energy Constant $C = 3.067$

REFERENCES

Beevi, A. S. and Sharma, R. K. (2012). Oblateness effect of Saturn on periodic orbits in the Saturn-Titan restricted three-body problem, Astrophys. Space Sci., Vol. 340, pp. 245–261.

Chandre, C., Wiggins, S. and Uzer, T. (2003). Time-Frequency analysis of chaotic systems, Physica D, Vol. 181, pp. 171–196.

Deplart, N., Escudie, B., Guillemain, P., Kronland Martinet, R., Tchamichian, P. and Torresani, B. (1992). Asymptotic wavelet and Gabor analysis, extraction of instantaneous frequency, IEEE Trans. on Information Theory, Vol. 38, No. 2, pp. 644–664.

Euaggelos E. Zotos (2015). How does the oblateness coefficient influence the nature of orbits in the restricted three-body problem, Astrophys. Space Sci., Vol. 358, pp. 33.

Freistetter, F. (2000). Fractal Dimensions as Chaos Indicators, Celestial Mechanics and Dynamical Astronomy, Vol. 78, pp. 1–4, 211–225.

Gupta Beena R and Kumar V. (2015). Time-Frequency Analysis of asymmetric triaxial galactic model including effect of spherical dark halo component, Int. J. Astron. and Astrophys., Vol. 5, pp. 106–115.

Gupta, Beena R. and Kumar, Vinay (2016). Characterization of the phase space structure of the Circular Restricted Three-Body Problem, Int. J. of Bifurcation and Chaos, Vol 26, No. 2, 1650029, pp. 1–13.

Kalantonis, V. S., Markellos, V. V. and Perdios, E. A. (2005). Computing periodic orbits of the three-body problem: Effective convergence of Newtons method on the surface of section, Astrophys. Space Sci., Vol. 298, pp. 441–451.

Kalantonis, V. S., Douskos, C. N. and Perdios, E. A. (2006). Numerical determination of homoclinic and heteroclinic orbits as collinear equilibria in the restricted three-body problem with oblateness, Celest. Mech. Dyn. Astron., Vol. 94, pp. 135–153.

Kalantonis, V. S., Perdios, E. A. and Perdiou, A. E. (2008). The Sitnikov family and the associated families of 3D periodic orbits in the photogravitational RTBP with oblateness, Astrophys. Space Sci., Vol. 315, pp. 323–334.

Kalvouridis, T. and Gousidou-Koutita, M. Ch. (2012). Basins of attraction in the Copenhagen problem where the primaries are magnetic dipoles, Applied Mathematics, Vol. 3, pp. 541–548.

Markellos, V. V., Papadakis, K. E. and Perdios, E. A. (1996). Non-linear stability zones around triangular equilibria in the plane circular restricted three-body problem with oblateness, Astrophys. Space Sci., Vol. 245, pp. 157–164.

Markellos, V. V., Roy, A. E., Velgakis, M. J. and Kanavos, S. S (2000). A photogravitational Hill problem and radiation effects on Hill stability of orbits, Astrophys. Space Sci., Vol. 271, pp. 293–301.

Matlab and Statistics Toolbox Release. (2010), *The MathWorks, Inc.*, Natick, Massachusetts, United States.

Michtchenko, T. A and Nesvorny, D (1996). Wavelet analysis of the asteroidal resonant motion, Astron. Atrophys, Vol. 313, pp. 674–678.

Perdiou, A. E., Perdios, E. A., Kalantonis, V. S.(2012). Periodic orbits of the Hill problem with radiation and oblateness, Astrophys. Space Sci., Vol. 342, pp. 19–30.

Pourtakdoust Seid H. and Sayanjali M. (2014). Fourth body gravitation effect on the resonance orbit characteristics of the restricted three-body problem, Nonlinear Dynamics, Vol. 76, No. 2, pp. 955–972.

Racoveanu, O (2014). Comparison of chaos detection methods in the circular restricted three-body problem, Astron. Nachr., Vol. 335, No. 8, pp. 877–885.

Saha, L. M., Das M. K., Narang P. and Yuasa M. (2008). On particle trajectories in restricted 3-body problem including the effect of radiation: Sun-Jupiter system, Astrophys Space Sci., Vol. 314, pp. 59–71.

Sharma, R. K., and Subba Rao, P. V., (1976). Stationary solutions and their characteristic exponents in the restricted three-body problem when the more massive primary is an oblate spheroid, Celest. Mech., Vol. 13, pp. 137–149.

Sharma, R.K. and Subba Rao, P.V. (1979). Effect of oblateness on triangular solutions at critical mass, Astrophys. Space Sci., Vol. 60, pp. 247–250.

Kumar et al.: Numerical Simulation of the Phase Space of Jupiter-Europa

AAM: Intern. J., Vol. 12, Issue 1 (June 2017)   493

Sharma, R.K. (1981). Periodic orbits of the second kind in the restricted three-body problem when the more massive primary is an oblate spheroid, Astrophys. Space Sci., Vol. 76, pp. 255–258.

Sharma, R. K., Subba Rao, P. V. (1986). On finite periodic orbits around the equilibrium solutions of the planar restricted three-body problem, Astrophys. and Space Sci., Vol. 127, pp. 71–85.

Sharma, R. K. (1987). The linear stability of libration points of the photogravitational restricted three-body problem when the smaller primary is an oblate spheroid, Astrophys. Space Sci., Vol. 135, pp. 271–281.

Sharma, R. K. (1989). The periodic orbits of the second kind in terms of Giacaglias variables with oblateness, Earth Moon Planets, Vol. 45, pp. 213–218.

Sharma, R. K. (1990). Periodic orbits of the third kind in the restricted three-body problem with oblateness. Astrophys. Space Sci., Vol. 166, pp. 211–218.

Singh, J. and Leke, O. (2012). Equilibrium points and stability in the restricted three-body problem with oblateness and variable masses, Astrophys. Space Sci., Vol. 340, pp. 27–41.

Singh, J. and Leke, O. (2013). Effect of oblateness, perturbations, radiation and varying masses on the stability of equilibrium points in the restricted three-body problem, Astrophys. Space Sci., Vol. 344, pp. 51–61.

Stuchi, T. J. et al. (2008). Dynamics of a spacecraft and normalization around Lagrangian points in the Neptune-Triton system, Advances in Space Research, Vol. 42, No. 10, pp. 1715–1722.

Subba Rao, P. V. and Sharma, R. K. (1988). Oblateness effect on finite periodic orbits at L4. *In 39th Congress of the International Astronautical Federation (IAF-88-300)*, Bangalore, India.

Subba Rao, P. V. and Sharma, R. K. (1997). Effect of oblateness on the non-linear stability of L4 in the restricted three-body problem, Celest. Mech. Dyn. Astron., Vol. 65, pp 291–312.

Szebehely, V. (1967). *Theory of Orbits*, Academic Press, New York.

Todorovska, M. (2001). *Estimation of Instantaneous Frequency of Signals using the Continuous Wavelet Transform*, Dept. of Civil Eng., Univ. of Southern Calif., Tech. Rep.

Vela-Arevalo, L. V and Marsden, J. E. (2004). Time-frequency analysis of the restricted three-body problem: transport and resonance transitions, Class. Quantum Grav., S351–S375, pp. 21.

Wavelab, http://www-stat.stanford.edu wavelab

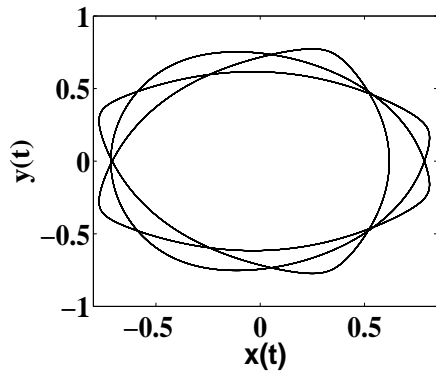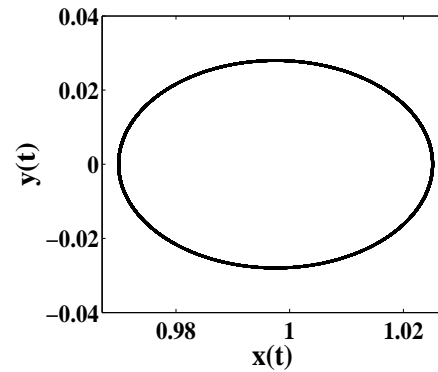Wolfram Research, Inc., Mathematica, Version 10.0, Champaign, IL (2014).
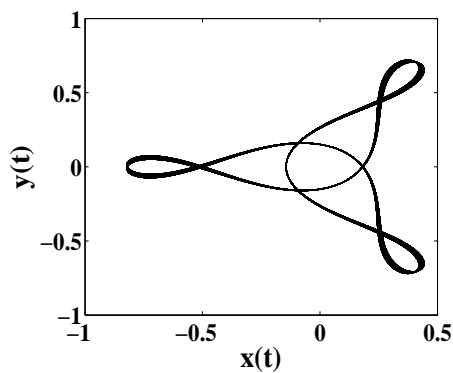
Appendix
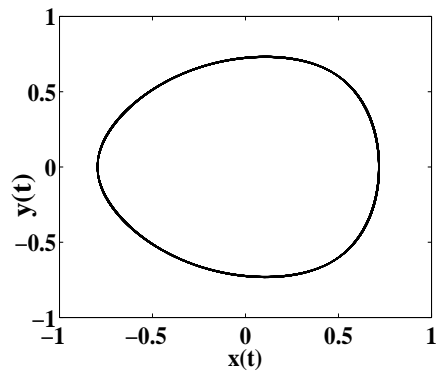
(a) Periodic orbit at (0.715, 0, 0, 0.4949)
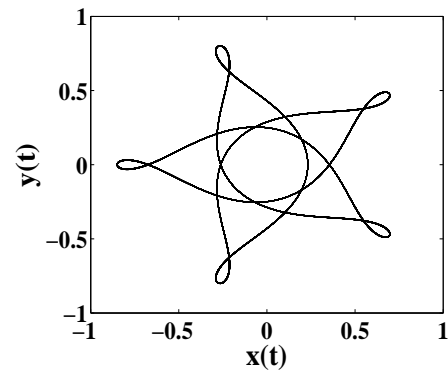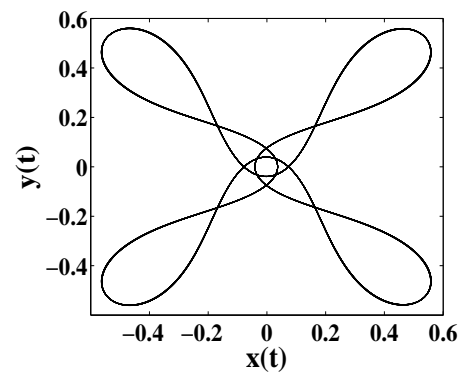
(b) Periodic orbit at (0.232, 0, 0, 2.3457)

(c) Periodic orbit at (0.619, 0, 0, 0.7361)

(d) Periodic orbit at (0.97, 0, 0, 0.3336)

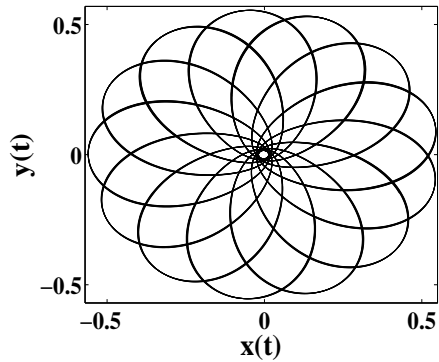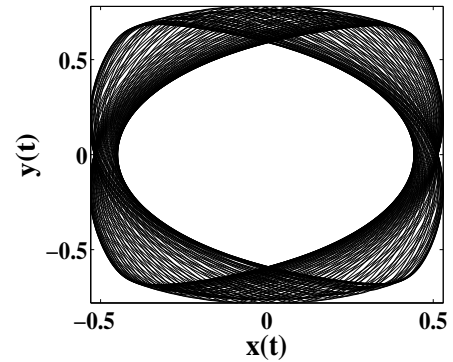(e) Periodic orbit at (-0.822, 0, 0, 0.2200)
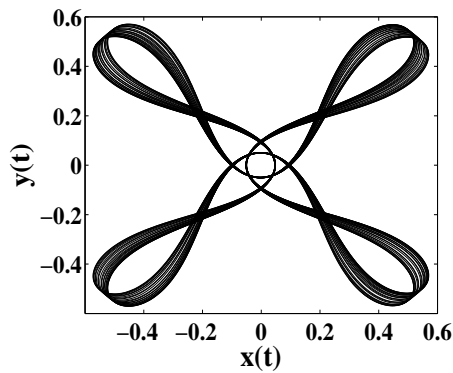
(f) Periodic orbit at (0.0364, 0, 0, 6.9425)

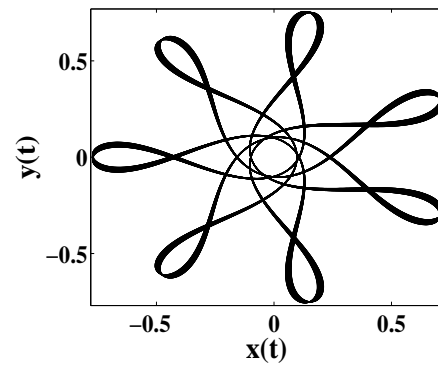Figure 16: Phase-portrait of different periodic orbits in the Jupiter-Europa system without oblateness effect

Kumar et al.: Numerical Simulation of the Phase Space of Jupiter-Europa

AAM: Intern. J., Vol. 12, Issue 1 (June 2017)   495

(a) Periodic Orbit at (-0.56, 0, 0, 0.8749)

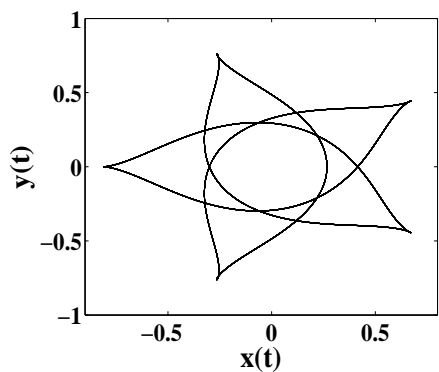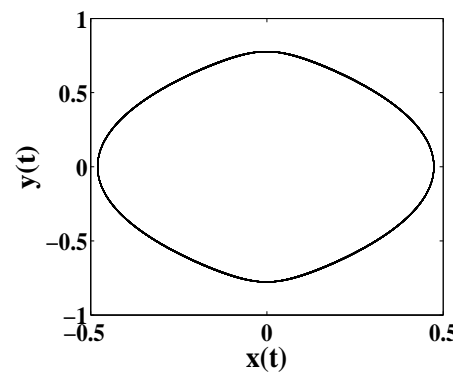(b) Periodic Orbit at (0.51, 0, 0, 1.0171)

(c) Periodic Orbit at (0.046, 0, 0, 6.1638)

(d) Periodic Orbit at (0.267, 0, 0, 2.0858)

(e) Periodic Orbit at (0.474, 0, 0, 1.1367)

(f) Periodic Orbit

Figure 17: Phase-portrait of different periodic orbits in the Jupiter-Europa system with oblateness effect